

Carbon-Nanotube–PDMS Composite Coatings on Optical Fibers for All-Optical Ultrasound Imaging

Sacha Noimark, Richard J. Colchester, Ben J. Blackburn, Edward Z. Zhang, Erwin J. Alles, Sebastien Ourselin, Paul C. Beard, Ioannis Papakonstantinou, Ivan P. Parkin, and Adrien E. Desjardins*

Polymer–carbon nanotube composite coatings have properties that are desirable for a wide range of applications. However, fabrication of these coatings onto submillimeter structures with the efficient use of nanotubes has been challenging. Polydimethylsiloxane (PDMS)–carbon nanotube composite coatings are of particular interest for optical ultrasound transmission, which shows promise for biomedical imaging and therapeutic applications. In this study, methods for fabricating composite coatings comprising PDMS and multiwalled carbon nanotubes (MWCNTs) with submicrometer thickness are developed and used to coat the distal ends of optical fibers. These methods include creating a MWCNT organogel using two solvents, dip coating of this organogel, and subsequent overcoating with PDMS. These coated fibers are used as all-optical ultrasound transmitters that achieve high ultrasound pressures (up to 21.5 MPa peak-to-peak) and broad frequency bandwidths (up to 39.8 MHz). Their clinical potential is demonstrated with all-optical pulse-echo ultrasound imaging of an aorta. The fabrication methods in this paper allow for the creation of thin, uniform carbon nanotube composites on miniature or temperature-sensitive surfaces, to enable a wide range of advanced sensing capabilities.

1. Introduction

Polymer–carbon nanotube composite coatings have broad applicability for sensing, including strain and pressure,^[1,2] chemical vapor and gas,^[3,4] and biomolecules.^[5–7] For many applications, methods to create and precisely deposit uniform composite coatings with micrometer-scale thicknesses and efficient use of carbon nanotubes remain a critical challenge. Accurate deposition onto submillimeter structures such as optical fibers is desirable for minimally invasive sensing applications, but common thin film deposition techniques such as spin coating^[8] and chemical vapor deposition (CVD) are not well suited for this. Inkjet printing can provide deposition over micrometer-scale regions, but achieving uniform deposition remains challenging due to “coffee-ring effects.”^[9–12]

Optical ultrasound transmission is emerging as a promising application of composite coatings for biomedical imaging, and polymer–carbon composites have been highlighted as particularly beneficial to optimize performance.^[13–19] Optical ultrasound transmission can be achieved with the photoacoustic effect, in which the absorption of pulsed light by an engineered material causes a pressure rise that propagates as an acoustic wave.^[20] For efficient conversion of optical to ultrasound energy, it is desirable to use materials with both high optical absorption and high thermal expansion coefficients.^[20] Composites with carbonaceous optical absorbers within polydimethylsiloxane (PDMS) elastomeric hosts fulfill these criteria and have resulted in particularly high conversion efficiencies.^[14–19] To date, these composites have been developed largely on planar surfaces.^[15–19]

Fiber-optic ultrasound transmitters are promising for interventional cardiology applications.^[21] PDMS–carbon nanotube composite coatings with thicknesses of $\approx 20 \mu\text{m}$ were achieved on the tips of optical fibers,^[14] which provided pressure amplitudes that were comparable to conventional electronic transmitters. Relative to conventional piezoelectric ultrasound transmission, optical transmission can provide broad bandwidths and comparable pressure amplitudes, without the complexity of electronic component assembly.^[13,14] However, to fully realize

Dr. S. Noimark, R. J. Colchester, Dr. E. Z. Zhang,
Dr. E. J. Alles, Prof. P. C. Beard, Dr. A. E. Desjardins
Department of Medical Physics and Biomedical
Engineering
University College London
Gower Street, London WC1E 6BT, UK
E-mail: a.desjardins@ucl.ac.uk

Dr. S. Noimark, B. J. Blackburn, Prof. I. P. Parkin
Materials Chemistry Research Centre
Department of Chemistry
University College London
20 Gordon Street, London WC1H 0AJ, UK

Prof. S. Ourselin
Center for Medical Imaging Computing
University College London
Gower Street, London WC1E 6BT, UK

Dr. I. Papakonstantinou
Department of Electronic and Electrical Engineering
University College London
Gower Street, London WC1E 6BT, UK

This is an open access article under the terms of the Creative Commons Attribution License, which permits use, distribution, and reproduction on any medium, provided that the original work is properly cited.

DOI: 10.1002/adfm.201601337



the potential of optical ultrasound transmitters for biomedical imaging, where a large range of ultrasound frequencies (high bandwidth) and large pressures amplitudes are required to achieve high resolution and sensitivity respectively, minimization of the composite coating thickness is essential.^[22,23] Indeed, it has been estimated that ultrasound attenuation in carbon–PDMS composites with high optical absorption increases dramatically with thickness, reaching nearly $1 \text{ dB } \mu\text{m}^{-1}$ at 100 MHz.^[23]

In this study, we developed methods for the creation of micrometer-scale multiwalled carbon nanotube (MWCNT)–PDMS composites with high optical absorption, on the distal end faces of optical fibers. These methods included the synthesis of a high concentration MWCNT formulation and a MWCNT organogel, which were deposited using one-step and multistep dip coatings. These composites were compared in terms of their performance as ultrasound transmitters and exhibited high ultrasound pressures with broad frequency bandwidths. To demonstrate their strong potential for use in biomedical ultrasound imaging, a fiber-optic transmitter was paired with a fiber-optic ultrasound receiver to create a miniature, flexible probe, and all-optical pulse-echo images of aortic tissue were acquired. The methods presented in this paper allow for the creation of thin, uniform carbon nanotube composites on miniature or temperature-sensitive surfaces, for a wide range of advanced sensing applications.

2. Results

2.1. MWCNT Coating Deposition and Characterization

High concentrations of MWCNTs dispersed in xylene (14 mg mL^{-1}) were achieved using the oleylamine functionalized-

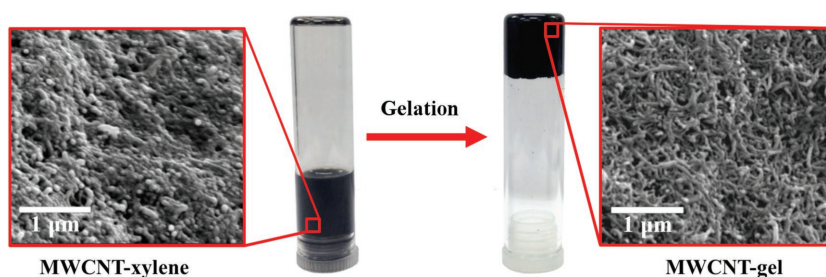


Figure 1. Synthesized functionalized MWCNT-xylene and MWCNT-organogel coating formulations and SEM images of the resultant MWCNT films on a planar glass substrate (insets).

pyrene ligand. This MWCNT dispersion was stable for more than 6 months. Addition of acetone resulted in the formation of a MWCNT-organogel, which was stable at room temperature (Figure 1).

Dip-coating deposition methods were used to deposit three MWCNT–PDMS composite materials onto the distal ends of optical fibers. The coatings differed significantly in their morphologies and optical opacities, as observed with light microscopy. With surface illumination, the MWCNT–PDMS integrated coating had a uniform, convex appearance across the fiber surface (Figure 2a) that contrasted with the nonuniform, concave appearance of the MWCNT-xylene coating (Figure 2b). With through-fiber illumination, the MWCNT-xylene/PDMS coatings were significantly more opaque to light at the edges than in the center (Figure 2b). This spatial pattern of the coating is characteristic of coffee-ring solvent drying effects where the thin coating at the center corresponds to the observed bright region. In contrast, the MWCNT-gel coating had a homogeneous appearance with both surface and through-fiber illumination, with no evidence of coffee-ring effects (Figure 2c).

The optical transmission spectra of all coatings across all fiber types were nearly uniform. Across measured wavelengths, optical absorption was greater than 94% for the

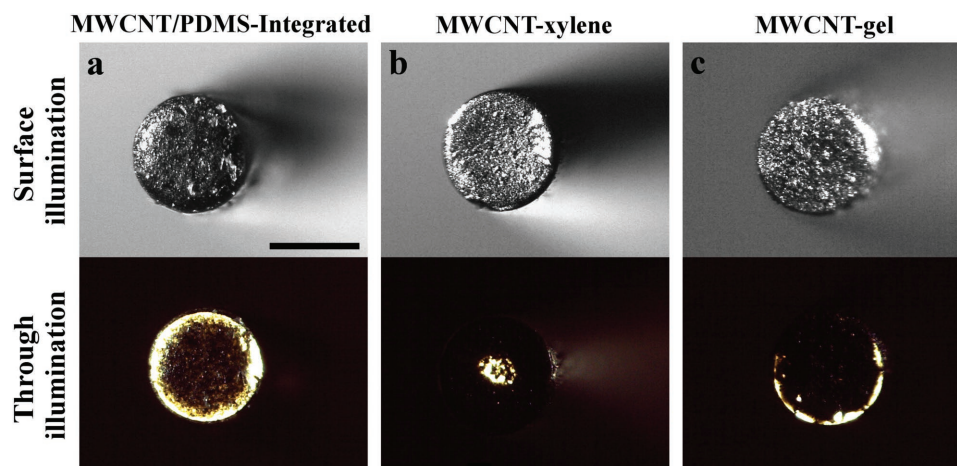


Figure 2. Distal end faces of optical fibers with three different MWCNT/PDMS coatings, either under dark conditions (top row) or illuminated through core (bottom row). a) Integrated MWCNT–PDMS-coated, b) MWCNT-xylene/PDMS-coated, and c) MWCNT-gel/PDMS-coated. In the bottom row, the bright regions in (a) and (c) correspond to the cladding, whereas the central bright region in (b) corresponds to “coffee-ring” staining effect. The exposure time was the same for each image. Scale bar: 200 μm .

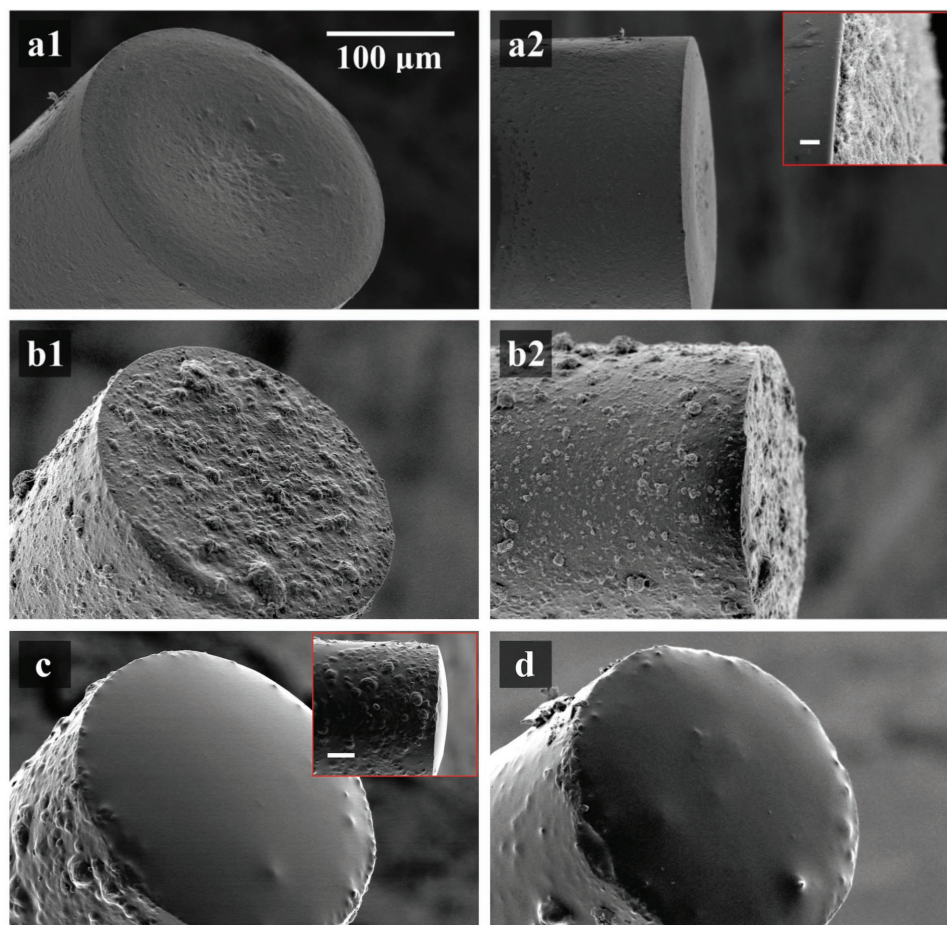


Figure 3. SEM images of coated 200 μm fibers. a1) MWCNT-xylene coating, a2) Side-view of MWCNT-xylene coating (inset, side-view, scale bar: 1 μm), b1) MWCNT-gel coating, b2) Side-view of MWCNT-gel coating, c) MWCNT-gel/PDMS coating (inset, side-view, scale bar: 50 μm), and d) MWCNT-PDMS integrated coating.

MWCNT-PDMS integrated coating and greater than 97% for both the MWCNT-xylene/PDMS and MWCNT-gel/PDMS bilayer coatings.

Significant differences in surface morphologies across the coatings were revealed by SEM imaging. The MWCNT-xylene coating had a dimple in the center which is characteristic of a coffee-ring pattern (Figure 3a1), but there appeared to be complete coverage of MWCNTs across the entire fiber end face (Figure 3a2). The MWCNT-gel coating was more uniform in its coverage than the MWCNT-xylene coating, although the former had greater surface roughness (Figure 3b1).

The high optical opacities of the MWCNT-xylene and MWCNT-gel coatings contrasted with the small coating thicknesses. Side-view SEM imaging indicated that the MWCNT-xylene coatings were less than 1 μm (Figure 3a2, inset); similar values were observed for the MWCNT-gel coatings, although there was greater variation in thickness across the fiber end faces (Figure 3b1,b2). Overcoating with PDMS resulted in domed surfaces (Figures 3c,d) that were typically 20 μm in maximum thickness, as observed with side-view SEM imaging (Figure 3c). The thickness of the integrated MWCNT-PDMS coating was also ≈ 20 μm . SEM imaging of fractured planar

surfaces revealed that the PDMS overcoat infiltrated the MWCNT-xylene and MWCNT-gel coating to reach the underlying glass surfaces, thereby forming composites (Figure 3d, Supporting Information).

The PDMS overcoat increased the mechanical robustness of the coatings. In its absence, the MWCNT-xylene and MWCNT-gel coatings were easily damaged by the application of tape (Scotch, 3M), or manual scratching using a stainless steel scalpel blade. All coatings with PDMS remained intact upon repeated application of tape and moderate applied scalpel pressure.

2.2. Ultrasound Performance and Imaging

2.2.1. Optical Ultrasound Generation

Ultrasound generated by the three coatings differed in terms of the peak-to-peak pressure amplitudes (Figure 4a). At a distance of 3 mm from the optical fiber end faces, the highest pressure amplitudes were achieved with the MWCNT-gel/PDMS coatings (1.36 MPa). By comparison, the amplitudes corresponding to the MWCNT-xylene/PDMS and the integrated

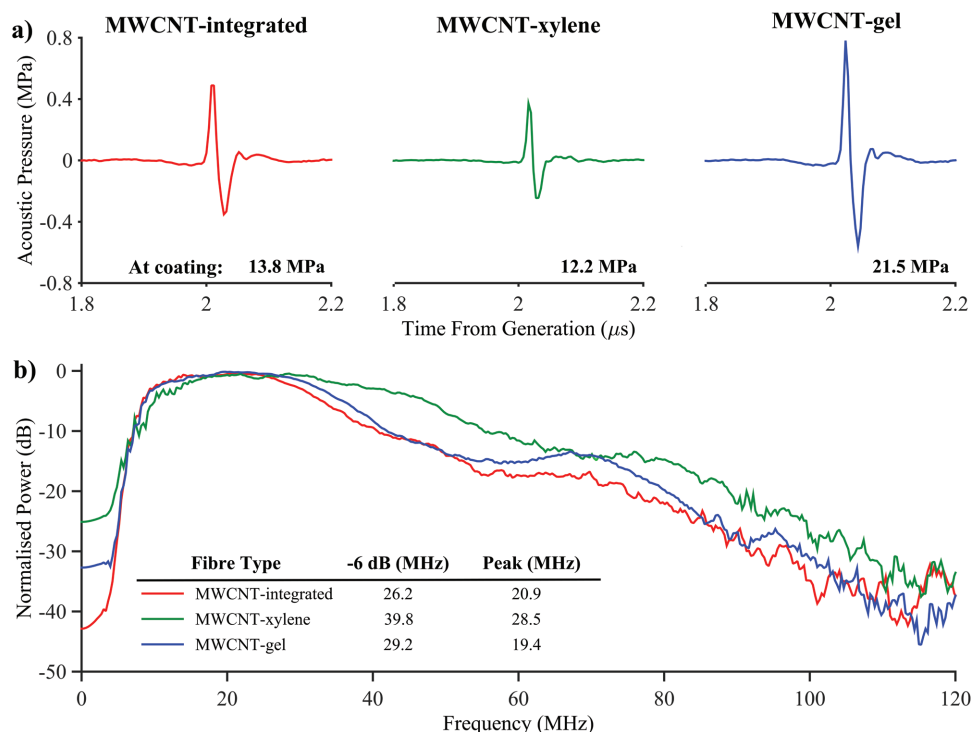


Figure 4. Ultrasound characterization of 200 μm core diameter optical fibers coated with: (i) MWCNT–PDMS integrated coating (red line), (ii) MWCNT–xylene/PDMS coating (green line), and (iii) MWCNT–gel/PDMS coating (blue line). a) Ultrasound pressures measured 3 mm from the end face of coated optical fibers and b) corresponding power spectra, with maximum pressures referenced to 0 dB.

MWCNT–PDMS coatings were 0.68 and 0.91 MPa, respectively. The peak-to-peak ultrasound pressures at the coating surfaces approached values used for high-intensity focused ultrasound, with 21.5 MPa achieved with the MWCNT-gel/PDMS coatings. The corresponding efficiencies of the integrated MWCNT–PDMS coating, the MWCNT-xylene/PDMS coating, and the MWCNT-gel/PDMS coatings were 0.37, 0.42, and 0.65 MPa $\text{mJ}^{-1} \text{cm}^{-2}$, respectively. For all three coatings a significant reduction in the transmitted ultrasound power was observed after reaching a threshold pressure of ≈ 4.5 MPa (Section 6.3, Supporting Information). Upon removal, there was no visible damage to the fibers and they functioned as previously at lower laser fluences. It is suspected that cavitation occurred due to the large negative pressures generated, obstructing transmission. The results for the three coating types were highly reproducible (Section 6.3, Supporting Information).

Whereas the MWCNT-xylene/PDMS coatings generated the smallest peak-to-peak pressure amplitudes, the bandwidth (39.8 MHz) and the peak frequency (28.5 MHz) were both the largest. The corresponding -6 dB bandwidths for the MWCNT-gel/PDMS and the integrated MWCNT–PDMS coatings were 29.2 and 26.2 MHz, respectively, with peak frequencies of 19.4 and 20.9 MHz.

Ultrasound pressures obtained from subsequent measurements using the same MWCNT/PDMS coated fibers under an identical irradiation regime were comparable, and visual inspection of the coatings showed no damage to fibers. The ultrasound signal level of all MWCNT/PDMS coated fibers was stable upon exposure to laser fluence for extended periods

of time (hours) and after multiple uses over a duration of 6 months.

With all-optical pulse-echo ultrasound imaging, the aorta was clearly visualized. Depth variations in the tissue morphology, including the tunica and the adventitia, could be observed and visualization extended through the vessel wall (Figure 5). The surface, which included a side-branch, was clearly delineated. Visualization of a side branch was achieved and visible as a hypochoic region.

3. Discussion

This study presented a new bilayer coating paradigm for fabricating carbon nanotube/PDMS composites with micrometer-scale thickness onto optical fibers, and demonstrated the use of these composites for optical ultrasound generation. The bilayer coating methods effectively achieved submicrometer thick, dense layers of MWCNTs (>97% absorption), with PDMS infiltration. This contrasts with CVD methods, where good PDMS integration is only achievable by growing sparser, less absorbing ($\approx 80\%$) nanotube films; PDMS cannot infiltrate thick, vertically aligned nanotube forests, resulting in poor heat transfer between the nanotubes and PDMS.^[16] One key advantage of the bilayer coating methods is the efficiency with which the carbon nanotubes are used. By comparison, with the integrated MWCNT–PDMS coatings, the nanotubes within the coating formulation that are not deposited onto the optical fiber become unusable once curing takes place.

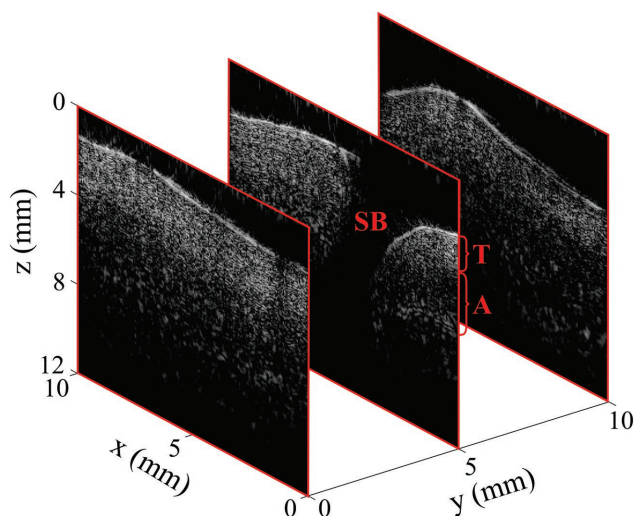


Figure 5. All-optical ultrasound cross-sections of swine aorta. Transmission was performed with a MWCNT-gel/PDMS coating; reception, with a Fabry–Pérot cavity. The tunica (T) and adventitia (A) are evident in all cross-sections (x : lateral distance; z : depth), and a side branch (SB) is visible in the middle one. The cross-sections were separated in the out-of-plane dimension (y) by 5 mm.

Efficient use of nanomaterials could make it practical to fabricate nanocomposites with exotic constituents such as high purity single-walled carbon nanotubes. Additionally, the bilayer coating methods may be advantageous from a biocompatibility standpoint, as the nanotubes are completely covered with the pure host polymer. These methods are a low-temperature, low-pressure alternative to CVD to achieve uniform, dense nanotube films on a variety of planar substrates (Figures 1 and 3, Supporting Information).

These results have applicability beyond optical fibers and optical ultrasound generation. Achieving dip-coating with an absence of coffee-ring effects is important in inkjet printing, where droplet surface morphology control is paramount.^[9–12,24] Coffee-ring stains result from a rapid solvent evaporation rate at the droplet boundary, which cause a convective flow of particles from the center, toward the drying edge.^[12] Opposing “Marangoni” flows can be used to recirculate the solvent within the drying droplet and redistribute particles to the droplet center, reducing coffee-ring staining.^[12] The MWCNT-gel formulation developed in this study exploits a two solvent, high boiling point–low boiling point system to help balance the two opposing flows and minimize coffee-ring coating effects, to achieve optically homogeneous coatings at the end face of the optical fibers. This MWCNT-gel technology has strong potential for use in inkjet printing and, could also be readily translated to larger surfaces such as those used for high-intensity focused ultrasound.^[15]

Miniaturization of imaging technologies is crucial for the advancement of minimally invasive surgical procedures such as cardiovascular interventions and minimally invasive fetal surgery. Varying the homogeneity and thickness of the MWCNT layer in the composite coatings resulted in three miniaturized all-optical ultrasound transmitters that demonstrated high ultrasound pressures and imaging resolution. Importantly,

transmitters with bilayer composite coatings performed better in terms of bandwidths and ultrasound pressures than integrated coatings. These thinner, strongly absorbing composites are more effective at optical ultrasound generation, since attenuation within the coating is minimized, particularly at high ultrasound frequencies.^[22,23]

To the authors’ knowledge, the MWCNT-gel/PDMS composite material in this study yielded the largest peak-to-peak ultrasound pressures for optical fiber coatings to date, with efficiencies of up to $0.65 \text{ MPa (mJ}^{-1} \text{ cm}^{-2})$ (surface acoustic pressure to laser energy). These high pressures are likely due to the uniformity of the MWCNTs across the optical fiber core for uniform optical absorption (MWCNT-gel/PDMS coating), and the small thickness of the nanotube–PDMS composite region for low ultrasound attenuation (MWCNT-xylene/PDMS coating). Higher efficiencies have been achieved with coatings on large, planar surfaces,^[17,19] which can be applied using techniques such as spin-coating that are not well suited to optical fibers. The ultrasound bandwidths achieved in this study were larger than most previously obtained with PDMS–carbon composites,^[14,15,17,19] which is important for achieving high spatial resolution. One exception can be found in the study of Vannacci et al., which yielded bandwidths beyond 150 MHz using coatings on optical fibers;^[25] however, the authors raised concerns about the degradation of their coatings with time.^[25] For the bilayer coatings in this study, improvements in bandwidth could be likely achieved by minimizing the thickness of the excess PDMS layer that overlies the composite. For the integrated coatings, decreasing the PDMS thickness while maintaining a constant optical absorption would require increasing the MWCNT concentration; challenges include limits on the achievable concentrations and reductions in the mechanical integrity of the coatings. Ultra-sonication of the MWCNT formulations may also yield additional performance improvements to both integrated and bilayer coatings, which might result from better MWCNT dispersibility and enhanced homogeneity of the MWCNT–PDMS composite solution (Section 6.3, Supporting Information).

The MWCNT/PDMS ultrasound transmitters fabricated in this study did not degrade with prolonged continuous use (as observed during the 4 h image acquisition time period) and exhibited good mechanical stability upon extensive use on tissues *ex vivo*. The results of the adherence and scratch tests are promising for the targeted use of these miniaturized ultrasound transducers for guiding minimally invasive procedures, where it is imperative that the coatings are not damaged and adhere well to the optical fiber. Infiltration of PDMS through the MWCNT network to the underlying glass substrate was likely important for promoting strong adhesion of the composite coating to the fiber tip.

The all-optical pulse-echo images of swine aorta were striking in terms of the detail that they showed, their imaging depth, and their spatial resolution. With their small size and high flexibility, these optical ultrasound transmitters can readily be integrated into medical devices for improved image-based guidance of minimally invasive procedures. When paired with fiber optic ultrasound receivers, miniature fiber optic ultrasound transmitters could also find applicability in intravascular imaging, to guide the placement of stents in

the coronary and carotid arteries. With their small dimensions and their inherent MRI compatibility, all-optical ultrasound is promising as an alternative to conventional intravascular ultrasound imaging. Visualization of side branches of the aorta could be valuable for guiding the placement of abdominal aortic aneurysm stents, where identification of the renal arteries can be of critical clinical importance. Accurate control of the deposition of carbon-PDMS composites onto temperature-sensitive surfaces with an efficient use of carbon nanostructures will enable the development of a new generation of medical devices.

4. Conclusion

This study reports the fabrication of three all-optical ultrasound transmitters, using a scalable strategy for the efficient deposition of MWCNT/PDMS composites onto micrometer-scale substrates, with minimized wastage of expensive nanomaterials. This coating technology is of broad interest, not only detailing a new MWCNT-formulation to overcome coffee-ring features, but presenting a simple route to coat larger substrates with highly absorbing, micrometer-scale composites. The ultrasound transmitters achieved strong ultrasound pressures for large tissue penetration depths, and wide bandwidths for high-resolution imaging. Pulse-echo imaging studies demonstrated their high performance, providing visualization of a high level of clinically relevant detail throughout the depth of swine aorta tissue. The combined resolution, penetration depths, and quality of the tissue images demonstrate the potential of this technology, with applications in guiding minimally invasive procedures such as vascular and intracardiac interventions.

5. Experimental Section

Synthesis and Coating Deposition: Three MWCNTs coating formulations were prepared. For each of them, the starting point was the synthesis of oleylamine-functionalized pyrene^[14,26] to functionalize MWCNTs (6–9 nm × 5 μm, Sigma Aldrich, UK) and thereby facilitate their dispersion in xylene (14 mg mL⁻¹), a solvent compatible with PDMS. This dispersion in xylene constituted the “MWCNT-xylene” coating formulation, and it was also used to create the “MWCNT-gel” coating formulation, by sonication with acetone (VWR, UK) in a 2:1 MWCNT-xylene:acetone ratio. The latter formed a gel when it rested overnight at room temperature. To prepare the “integrated MWCNT–PDMS” coating formulation, the MWCNT-xylene coating formulation (1.3 mL) was manually mixed with xylene (0.5 mL) and PDMS (1 g, MED-1000, Polymer Systems Technology, UK) and used immediately due to rapid polymer curing.

The three MWCNT coating formulations were applied to the distal ends of optical fibers using dip-coating (Figure 6) and for each coating type, three coated fibers were prepared. Multimode optical fibers (step-index, silica-core/silica-cladding; core/cladding diameter 200/220 μm) were mechanically stripped of buffer layers and cleaved perpendicular to their axes. Each optical fiber was then inserted into one of the three coating formulations (MWCNT-xylene; MWCNT-gel;

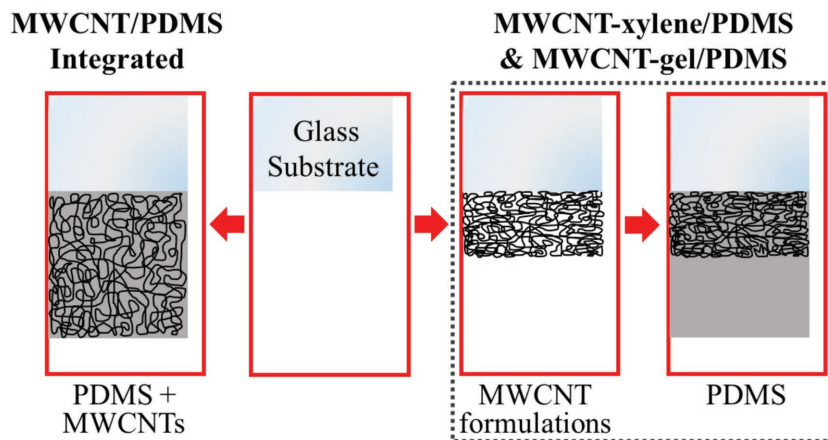


Figure 6. Schematic of dip-coating methods for bilayer and integrated MWCNT/PDMS coatings. For integrated coatings, the substrate is dipped into a functionalized MWCNT-PDMS composite solution. For bilayer coatings, the glass substrate is dipped into a functionalized MWCNT-formulation (MWCNT-xylene or MWCNT-gel formulation) and subsequently dipped into a PDMS solution.

MWCNT-PDMS), held stationary (20 s) and subsequently withdrawn (6 cm min⁻¹). To create bilayer coatings, which were termed “MWCNT-xylene/PDMS” and “MWCNT-gel/PDMS,” the MWCNT-xylene and MWCNT-gel coated optical fibers were dried (1 h) and subsequently dip-coated with a PDMS solution in xylene (1 g PDMS:1.8 mL xylene). For all three coatings, the PDMS was cured at room temperature (24 h). Consistency of the coating deposition method was tested (Section 6, Supporting Information).

While coating the distal ends of optical fibers was the primary focus of this study, the integration of PDMS within the MWCNT-xylene and MWCNT-gel coatings was tested using glass microscope cover slips. Each glass cover slip was dipped in one of those two coating formulations (20 s), withdrawn (6 cm min⁻¹) and air dried (1 h). Half of these coatings were subsequently postcoated with PDMS (1 g:1.8 mL xylene), which was cured at room temperature (24 h).

Materials Characterization and Functional Testing: The optical absorption of the composite coatings on the distal ends of optical fibers was measured across the wavelength range of 400–1300 nm. Broadband light from a halogen lamp (HL-2000-FHSA-LL, Ocean Optics, FL, USA) was delivered from the proximal end of a fiber; transmitted light at the distal end was received by an integrating sphere (FOIS-1, Ocean Optics, USA) and measured with two spectrometers (Maya2000 Pro (500–1000 nm) and NIRQuest512 (900–1300 nm), Ocean Optics, USA). A noncoated, cleaved optical fiber was used as a wavelength-independent reference and a dark measurement was obtained to correct for background spectrometer signals.

Scanning electron microscopy (SEM) of the composites on the distal ends of optical fibers was performed using secondary electron imaging on a field emission instrument (JSM-6301F, JEOL, Japan) with an acceleration voltage of 5 kV.

Ultrasound Characterization and Imaging: Ultrasound was generated with pulsed laser light, with a pulse width of 2 ns and a wavelength of 1064 nm (SPOT-10-500-1064, Eforlight, UK). The pulse energy delivered to the coating was 10.4 μJ, with a corresponding fluence of 33.1 mJ cm⁻².

Ultrasound pressure measurements were performed with the distal end of the optical fiber submerged in a water bath. Time-resolved ultrasound pressure measurements at multiple spatial locations were obtained with a bulk planar Fabry–Pérot sensor that was previously described by Zhang et al.^[27] This sensor was interrogated using a continuous wave, tunable laser (Tunics T100S-HP CL, Yenista Optics, France) operated in the wavelength range of 1500–1550 nm; measurements were made across a grid of 10 mm × 10 mm with a

spacing of 50 μm . The distal end of the optical fiber was 3 mm from the sensor surface. These spatially resolved measurements were used to calculate the ultrasound pressure at the distal end face of the optical fiber, using numerical back-propagation.^[28] Bandwidths were measured with a piezoelectric membrane hydrophone receiver (400 μm element) that was calibrated from 1 to 60 MHz (Precision Acoustics, UK), which was positioned at a distance of 3 mm along the axis of the optical fiber.

All-optical pulse-echo ultrasound imaging was performed with a miniature probe that comprised two fibers in apposition: one for transmission and another for reception. The optical fiber used for transmission had a MWCNT-gel/PDMS coating; the one used for reception had a Fabry–Pérot cavity.^[29] This probe was mounted on a motorized two-axis translation stage (Thorlabs, MTS50/M-Z8E). Each line scan was obtained with linear probe translation over a 10 mm distance, with spacing of 50 μm between depth scans. Three line scans were obtained, which were separated by 5 mm in a direction orthogonal to the probe translation. At each point, ultrasound was generated and the signal obtained from the Fabry–Pérot cavity was sampled at 250 MS s⁻¹ (M41.4420-X8, Spectrum, Germany). The data were preprocessed using a method described previously by Colchester et al.,^[13] and reconstructed as a 2D image using the MATLAB k-Wave toolbox.^[30] The sample was a section of swine aorta ex vivo, which was cut along the longitudinal axis and affixed to a cork ring to expose the inner lumen surface.

Supporting Information

Supporting Information is available from the Wiley Online Library or from the author.

Acknowledgements

This work was supported by an Innovative Engineering for Health award by the Wellcome Trust (No. WT101957) and the Engineering and Physical Sciences Research Council (EPSRC) (No. NS/A000027/1), by a Starting Grant from the European Research Council (ERC-2012-StG, Proposal No. 310970 MOPHIM), and by an EPSRC First Grant (No. EP/J010952/1).

Received: March 15, 2016

Revised: July 25, 2016

Published online:

- [1] S. Pyo, J. I. Lee, M. O. Kim, T. Chung, Y. Oh, S. C. Lim, J. Park, J. Kim, in *Transducers & Eurosensors XXVII: The 17th Int. Conf. on Solid-State Sensors, Actuators and Microsystems*, IEEE, Piscataway, NJ **2013**, pp. 1004–1007.
- [2] G. Yin, N. Hu, Y. Karube, Y. Liu, Y. Li, H. Fukunaga, *J. Compos. Mater.* **2011**, *45*, 1315.
- [3] C. Wei, L. Dai, A. Roy, T. B. Tolle, *J. Am. Chem. Soc.* **2006**, *128*, 1412.
- [4] S. M. Cho, Y. J. Kim, Y. S. Kim, Y. Yang, S. C. Ha, in *Proc. IEEE Sensors*, Vol. 2, IEEE, Piscataway, NJ **2004**, pp. 701–704.
- [5] X. Luo, A. J. Killard, A. Morrin, M. R. Smyth, *Anal. Chim. Acta* **2006**, *575*, 39.
- [6] J. Li, E. C. Lee, *Biosens. Bioelectron.* **2015**, *71*, 414.
- [7] S. C. Tsai, Y. C. Li, S. W. Liao, *Biosens. Bioelectron.* **2006**, *22*, 495.
- [8] D. J. Lipomi, R. V. Martinez, M. A. Kats, S. H. Kang, P. Kim, J. Aizenberg, F. Capasso, G. M. Whitesides, *Nano Lett.* **2011**, *11*, 632.
- [9] H. Hu, R. G. Larson, *J. Phys. Chem. B* **2006**, *110*, 7090.
- [10] R. Tortorich, J. W. Choi, *Nanomaterials* **2013**, *3*, 453.
- [11] E. Tekin, P. J. Smith, U. S. Schubert, *Soft Matter* **2008**, *4*, 703.
- [12] S. Y. Cho, J. M. Ko, J. Lim, J. Y. Lee, C. Lee, *J. Mater. Chem. C* **2013**, *1*, 914.
- [13] R. J. Colchester, E. Z. Zhang, C. A. Mosse, P. C. Beard, I. Papakonstantinou, A. E. Desjardins, *Biomed. Opt. Express* **2015**, *6*, 1502.
- [14] R. J. Colchester, C. A. Mosse, D. S. Bhachu, J. C. Bear, C. J. Carmalt, I. P. Parkin, B. E. Treeby, I. Papakonstantinou, A. E. Desjardins, *Appl. Phys. Lett.* **2014**, *104*, 1.
- [15] H. W. Baac, J. G. Ok, A. Maxwell, K. T. Lee, Y. C. Chen, A. J. Hart, Z. Xu, E. Yoon, L. J. Guo, *Sci. Rep.* **2012**, *2*, 989.
- [16] H. W. Baac, J. G. Ok, T. Lee, L. J. Guo, *Nanoscale* **2015**, *7*, 14460.
- [17] B. Y. Hsieh, J. Kim, J. Zhu, S. Li, X. Zhang, Xi. Jiang, *Appl. Phys. Lett.* **2015**, *106*, 021902.
- [18] H. Won Baac, J. G. Ok, H. J. Park, T. Ling, S. L. Chen, A. J. Hart, L. J. Guo, *Appl. Phys. Lett.* **2010**, *97*, 234104.
- [19] W. Y. Chang, W. Huang, J. Kim, S. Li, X. Jiang, *Appl. Phys. Lett.* **2015**, *107*, 161903.
- [20] B. T. Cox, P. C. Beard, *J. Acoust. Soc. Am.* **2005**, *117*, 3616.
- [21] G. van Soest, E. Regar, A. F. W. van der Steen, *Nat. Photonics* **2015**, *9*, 626.
- [22] M. O'Donnell, Y. Hou, J. S. Kim, S. Ashkenazi, S. W. Huang, L. J. Guo, *Eur. Phys. J. Spec. Top.* **2008**, *153*, 53.
- [23] T. Buma, M. Spisar, M. O'Donnell, *IEEE Trans. Ultrason., Ferroelectr. Freq. Control* **2003**, *50*, 1161.
- [24] D. Soltman, V. Subramanian, *Langmuir* **2008**, *24*, 2224.
- [25] E. Vannacci, L. Belsito, F. Mancarella, M. Ferri, G. P. Veronese, A. Roncaglia, E. Biagi, *Biomed. Microdev.* **2014**, *16*, 415.
- [26] S. Majeed, V. Filiz, S. Shishatskiy, J. Wind, C. Abetz, V. Abetz, *Nanoscale Res. Lett.* **2012**, *7*, 296.
- [27] E. Zhang, J. Laufer, P. Beard, *Appl. Opt.* **2008**, *47*, 561.
- [28] X. Zeng, R. J. McGough, *J. Acoust. Soc. Am.* **2009**, *125*, 2967.
- [29] E. Z. Zhang, P. C. Beard, *Proc. SPIE* **2015**, 9323.
- [30] B. E. Treeby, B. T. Cox, *J. Biomed. Opt.* **2010**, *15*, 021314.